Hydrogen Concentrations on C-class Asteroids from Remote Sensing

A. S. Rivkin[1,*], J. K. Davies[2,*], J. R. Johnson[3,*], S. L. Ellison[4,*], D. E. Trilling[5,*], R. H. Brown[6] L. A. Lebofsky[6]

August 19, 2003

1. Massachusetts Institute of Technology, 77 Massachusetts Avenue, Cambridge MA 02139

2. UK Astronomy Technology Centre, Royal Observatory Edinburgh, Edinburgh EH9 3HJ, UK

3. USGS Astrogeology Team, Flagstaff AZ 86001

4. Departamento de Astronomia, P. Universidad Catolica de Chile, Casilla 306, Santiago 22, Chile, and European Southern Observatory, Casilla 19001, Santiago 19, Chile

5. University of Pennsylvania, Department of Physics and Astronomy, David Rittenhouse Laboratory, 209 S. 33rd St., Philadelphia, PA 19104

6. Department of Planetary Sciences, University of Arizona, Tucson AZ 85721

Abstract:

We present spectroscopic observations of 16 asteroids from 1.9–3.6 μm, collected from the United Kingdom Infrared Telescope (UKIRT) from 1996–2000. Of these 16 asteroids, 11 show some evidence of a 3-μm hydrated mineral absorption feature greater than 2 σ at 2.9 μm. Using relations first recognized for carbonaceous chondrite powders by Miyamoto and Zolensky (1994) and Sato *et al.* (1997), we have determined the hydrogen:silicon ratio for these asteroids and calculated their equivalent water contents, assuming all the hydrogen was in water. The asteroids split into two groups, roughly defined as equivalent water contents of greater than $\sim$ 7% (eight asteroids, all with 3-μm band depths greater than $\sim$ 20%) and less than $\sim$3% (the remaining eight asteroids). This latter group includes some asteroids for which there is a small but statistically significant 3-μm band of non-zero depth. The G-class asteroids in the survey have higher water contents, consistent with CM chondrites. This strengthens the connection between CM chondrites and G asteroids that was proposed by Burbine (1998). We find that the 0.7-μm and 3-μm band depths are correlated for the population of target objects.

1 Background and Previous Work

The presence of water- and hydroxyl-bearing minerals (hereafter called "hydrated minerals") in meteorites and asteroids is long-established (DuFresne and Anders, 1962; Lebofsky, 1978; Lebofsky, 1980). Given the importance of asteroid impacts as a source of water to the early Earth (Delsemme, 2000; Morbidelli *et al.*, 2000) and the possible use of asteroids for resource utilization purposes (Lewis *et al.*, 1993), quantifying the amount of water present in the asteroid population is critical. We present a means of making a quantitative assessment of the H/Si ratio on C-class asteroid surfaces using remote sensing (Section 4). First, however, we review both asteroid taxonomy as is appropriate to this work and previous studies of hydrated minerals on asteroids (Sections 1.1, 1.2). We describe our observations and data reduction in Sections 2 and 3. We consider implications of the data and calculated H/Si ratios in Section 5. Finally, a discussion of future work can be found in Section 6.

1.1 C-class asteroids: Taxonomies

The spectral taxonomy for asteroids of Tholen (1984) defined a large C taxon, subdivided into "C" "B", "F", and "G" subclasses. These have been interpreted as related to each other via differing amounts of alteration of a common progenitor material, probably related to carbonaceous chondrite meteorites (Gaffey *et al.*, 1989). In this taxonomy, 1 Ceres is a G-class asteroid, and 2 Pallas is a B-class asteroid.

The taxonomy of Bus and Binzel (2002) includes much of the Tholen terminology wherever possible to maintain consistency. They have a large "C complex", with a variety of subclasses (B, C, Cb, Cg, Ch, Cgh). In this taxonomy, for comparison, 1 Ceres is a C-class asteroid, while 2 Pallas remains a B-class asteroid.

All of the asteroids included in this work have been classified in one of the C-subclasses by both Tholen and Bus and Binzel with two exceptions: 375 Ursula was classified as C-class by Tholen, but Xc by Bus and Binzel. The Xc-class is "next door" to the C-complex in principal component space, however. The other exception is somewhat more serious: 980 Anacostia was classified as SU by Tholen, and as L by Bus and Binzel. It is included here because it may have some affinity to the CV/CO meteorites (Burbine *et al.*, 1992), and thus belongs in a discussion of carbonaceous chondrite analogs. The spectral classifications for the target asteroids in both the Bus and Binzel and Tholen taxonomies is found in Table 1.

1.2 Hydrated Minerals on C-class Asteroids

Hydrated minerals give rise to absorptions throughout the infrared spectral region. The strongest absorptions occur near 3 μm, where features due to OH vibrational fundamentals (~ 2.75 μm) as well as the first overtone of H_2O

(~ 3.1 μm) are found. The result is a broad absorption band stretching from 2.7–3.5 μm or beyond, which is generally referred to as the "3-μm band". Because the OH fundamental has its band minimum at a wavelength which is difficult to impossible to observe from the ground for objects of asteroidal brightness, the band depth for the 3-μm band on asteroids must be measured at a different wavelength. In this work, we measure the band depth at two wavelengths: 2.9 and 3.2 μm.

Lebofsky *et al.* (1981) concluded that 1 Ceres had a surface dominated by minerals similar to terrestrial montmorillonites, based on its 3-μm band shape. King *et al.* (1992) instead suggested ammoniated phyllosilicates as analogs for Ceres' surface. Larson *et al.* (1983) argued that 2 Pallas was roughly analogous to CI/CM meteorites based on a qualitative list of common spectral characteristics. A quantitative investigation of a larger population has not been made, however.

Feierberg *et al.* (1985) obtained 3-μm spectra of 14 C-class asteroids, finding correlations between band depth and UV absorption strength shortward of 0.4 μm and suggesting that the C class may consist of fragments of anhydrous, CV/CO3-like cores and hydrated, CI1- or CM2-like mantles. Jones *et al.* (1990) increased the sample size to 32 C-class asteroids, finding 66% of them to have hydrated silicate surfaces, and finding that the hydrated mineral abundances of C-class asteroids decline gradually from 2.5–3.5 AU. The work of Jones *et al.* and Feierberg *et al.* allowed the first reckoning of the hydration state of the C class as a whole. However, the instruments available in the 1980s were only able to provide a binary "yes/no" to hydration state rather than detailed, quantitative band depths and shapes for a large number of objects.

More recently, an absorption feature near 0.7 μm has been correlated with the 3-μm water of hydration feature by Vilas (1994) and Howell *et al.* (2001). Hiroi *et al.* (1996) used the relative strengths of the 0.7- and 3-μm bands to conclude the C asteroids suffered thermal metamorphism, as further discussed below. The taxonomy of Bus and Binzel (2002) append an "h" when the 0.7-μm band is found in C-class or -subclass asteroids. Again, this serves simply to inform that hydrated minerals do (or don't) exist rather than quantitatively interpreting them. Indeed, at this point the correlation between the depth of the 0.7-μm band and the amount of hydrated minerals is still under investigation (Howell *et al.*, 2001).

2 Observations

These data were taken using CGS4, a cooled grating array spectrometer, on the United Kingdom Infrared Telescope (UKIRT) from 1996-2000 (Mountain *et al.*, 1990). This spectrometer covers 0.67 μm per grating setting, so three settings (center wavelengths at 2.20, 2.76 and 3.23 μm) were used to cover the wavelength region of interest with sufficient overlap to allow for proper normalization. This resulted in coverage from 1.9–3.6 μm. The grating ranges, as well as a plot of the atmospheric transmission, can be found in Figure 1. Because the middle grating covers 2.45-3.10 μm simultaneously, including both sides of the spectral region unobservable due to telluric water, scaling of the $\lambda < 2.5$ μm and $\lambda > 2.9$ μm data to one another can be done in a straightforward manner. Some of the objects only had data taken through the two longer-wavelength gratings, resulting in 2.45–3.6 μm spectra.

Standard star observations were contiguous with asteroid observations. Each asteroid had a standard star chosen to be of roughly solar type (and main sequence when possible) and to minimize airmass differences. The standard stars used for each asteroid are also shown in Table 1. Because the $K - L$ colors for main sequence stars differ from solar by only 1-2% from F2 all the way to K1 (Koornneef, 1983) and all of the standard stars fall within that classification range, no further correction to solar colors was performed. For comparison, the Sun is a G2 star, in the middle of that stellar classification range.

In order to decrease observational uncertainties, the data, which originally had a spectral resolution of $\frac{\lambda}{\Delta\lambda} = 400$, were binned by a factor of 24 to a final resolution of 32-60. The science goals of searching for broad hydrated mineral absorption features and determining continuum levels in the 2.5-3.5 μm region were easily met at this resolution. The binning was done simply by dividing the data into 64 regions of 24 pixels each, and determining the new average and standard deviation for each 24-pixel region.

3 Thermal Flux Corrections

Longward of roughly 3 μm, the signal received from bodies in the asteroid belt contains both thermal and reflected components. Therefore, thermal corrections were calculated using the Standard Thermal Model (STM), described in Lebofsky and Spencer (1989) in order to determine the true reflectance spectrum. Models with beaming parameters (η) with values of 0.756, 0.85, 0.9, and 1.0 were calculated for each object, plus an additional model with η equal to 0.78 was calculated for 324 Bamberga. This range of model values for η roughly matches the values seen among main-belt asteroids. The larger values for η result in models with less predicted thermal flux. While the uncertainty in the thermal correction increases with wavelength, it is quite small at the wavelengths of greatest interest near 3 μm. Furthermore, because the thermal correction increases monotonically with wavelength throughout this spectral region (and well beyond), one cannot create a spurious local minimum by applying a thermal correction. The effect of using too small a value for η is to overestimate the contribution of thermal flux, and create a spectrum that decreases with increasing wavelength, which is not seen in meteorite samples. This effect is relatively obvious, and thus avoidable. The effect of using too large a value for η would conversely lead to a spectrum which increases with increasing wavelength. This case is somewhat more difficult to diagnose, since some objects have reflectances which truly do increase with increasing wavelength. An example of the effect of changing η upon thermal corrections is shown in Figure 2.

The value of η used for each asteroid was chosen by inspection of the resulting spectrum, with the selected values (as well as values for albedo and diameter from Tedesco *et al.*, 1992, Millis *et al.*, 1984, and Storrs *et al.*, 1999) shown in Table 2. These values were selected such that the behavior at 3.6 μm matched a continuum extrapolated from the 2.4-μm region. Where two thermal corrections seemed equally well-suited, the one with a larger η was selected because that used the smaller correction, at the potential cost of underestimating the band depth at 3.2 μm. The values of η which were chosen for the various asteroids spanned the entire range from 0.756 to 1.0. This is not wholly unexpected, since the beaming parameter is an abstraction of surface roughness, thermal inertia, and other properties which are difficult to model explicitly, and the range of beaming parameters among asteroids is seen to vary from 0.756 for Ceres and Pallas (Lebofsky *et al.*, 1986) to 1.2 for near-Earth asteroids (Harris, 1998). For some of our target asteroids (2 Pallas, 13 Egeria: see Figure 3), the long-wavelength continuum ($\sim$3.6 μm) falls below the level of short-wavelength continuum ($\sim$2.4 μm). This behavior is also seen in hydrated mineral spectra (Salisbury *et al.*, 1991), and so is again not unexpected.

4 Results

4.1 3-μm Band Depths and Band Shapes

Figure 3 shows the thermally-corrected spectra of the the target asteroids. The band depths at 2.9 and 3.2 μm (calculated as 1 - $\frac{R_\lambda}{R_{2.5}}$) are shown in Table 3. Eleven of them show evidence of a 3-μm absorption band with a greater than 2-σ detection at 2.9 μm. Four of the asteroids have no observable feature within 1 σ. Asteroid 704 Interamnia has an apparent 2.9 μm band at 9.3 $\pm$ 5.9%, or roughly 1.5 σ. This ratio of hydrated to anhydrous C-class asteroids ($\sim$ 2:1) has been seen in a number of other works (Jones *et al.*, 1990; Vilas, 1994), but we caution the reader that the sample of targets in this work was chosen partially on the basis of previous work, and so is not unbiased. Of the seven new objects presented here, three show no 2.9 μm feature greater than 1 σ, while four show 2-σ or greater features. Though a small sample, this too is in rough agreement with what would be expected. In general, the band shapes appear similar to each other where present, with a presumed band minimum in the spectral region obscured by the atmosphere and with reflectance increasing roughly linearly with wavelength beyond that. Two asteroids, 1 Ceres and 375 Ursula, have 3 μm band shapes that are more rounded, and do not fit this description. *None* of the target asteroids have an apparent "inverse" feature, which would be expected on some of the asteroids if the 3-μm feature were due to incomplete atmospheric correction. In no case is there a negative band depth greater than 1 σ at 2.9 μm, where imperfect atmospheric correction would have a large effect. Some of the values of band depth at 3.2 μm shown in Table 3 suggest a negative feature. However, these can all be explained by two factors: First, the decision to choose the smaller thermal correction when presented with two equally-good thermal models leads to a reflectance at 3.2 μm that is higher than it "should" be. Second, because the values for band depth in Table 3 assume a flat continuum beyond 2.5 μm, an object with a sloping continuum and little or no 3-μm band would have a reflectance at 3.2 μm higher than at 2.5 μm and a negative band depth.

The 3 μm band shapes can be roughly quantified using a plot first introduced by Sato *et al.* (1997). Figure 4 shows the 2.9-μm/2.5-μm reflectance ratio vs. the 3.2-μm/2.5-μm reflectance ratio for a number of carbonaceous chondrite spectra, as well as for the target asteroids. The meteorite data come from Hiroi *et al.* (1996). The meteorite data trend along a line on such a plot. The majority of target asteroids also fall along this linear trend. However, Ceres and Ursula are off the trend because of their unusual spectra in the 3-μm region. On this plot, anhydrous meteorites and asteroids fall near (1,1) or to the upper right of that point. The fact that the asteroids fall along the meteorite trend is consistent with their surfaces being similar in hydrated mineral composition.

4.2 Determining the Hydrogen/Silicon Ratio

Recent work in the field of meteorite studies has shown that it is possible to estimate the amount of water in an asteroidal regolith. Miyamoto and Zolensky (1994) showed that the integrated intensity of the 3-μm absorption band is correlated with the hydrogen/silicon ratio in carbonaceous chondrite powders. Later work by Sato *et al.* (1997) showed that the integrated intensity of the 3-μm band in carbonaceous chondrite powders is related to the ratio of the 2.9 μm (as well as the 3.2 μm) reflectance to 2.5 μm reflectance. We again stress that these ratios do not represent different absorption features, but band depths for the broad 3-μm band at two different wavelengths. Put together, one can determine the H/Si ratio remotely assuming the target surface is analogous to the powders used in the studies.

We performed a linear least-squares fit to the Miyamoto and Zolensky data, digitized from their Figure 4 to obtain an analytical expression for the H/Si ratio as a function of integrated intensity. Similarly, we fit both the 2.9- and 3.2-μm reflectance ratios as a function of integrated intensity, following Sato *et al.*. The fits to these data are shown in Figures 5 and 6. We then combined these two functions to get H/Si ratio as a function of the reflectance ratios:

$$\mathrm{H/Si} = 7.3806 - 7.2893 \times \frac{R_{2.9}}{R_{2.5}} \tag{1}$$

$$\mathrm{H/Si} = 11.8456 - 11.0743 \times \frac{R_{3.2}}{R_{2.5}} \tag{2}$$

We note that these relations are experimentally-based rather than derived from first principles. Furthermore, they will only hold for surfaces that are analogous to carbonaceous chondrite powders. Finally, the nature of reflectance spectroscopy is such that only the surface of the body is sensed (technically speaking only the top $sim10\mu$m or so, though mixing within the regolith should homogenize at least the top several centimeters, using the lunar regolith as a guide: Hörz *et al.*, 1991) . Thus, the H/Si ratio determined for the surface of an asteroid may be different from the bulk H/Si ratio for the entire body. It should be further noted that a band depth of zero does *not* mean that $\frac{R_{2.9}}{R_{2.5}}$ or $\frac{R_{3.2}}{R_{2.5}}$ is equal to one, because the continuum was not removed from the original Sato *et al.* (1997) data; also, the data do not all fall perfectly on the best-fit line. A body with no hydrogen would be calculated to have a $\frac{R_{2.9}}{R_{2.5}}$ value of 1.01, and a $\frac{R_{3.2}}{R_{2.5}}$ value of 1.07, using these equations.

Equations 1 and 2 were used to calculate the H/Si ratios and equivalent water contents for the target asteroids and control meteorites in Figures 7 and 8 below.

4.3 Equivalent Water Contents

In order to estimate water contents from the H/Si ratio, a value for bulk Si concentration is needed. This is provided for various meteorite classes in Jarosewich (1990). Given this number, the weight percentage of H can be determined. In order to maintain consistency with the tables of modal analyses given in geochemical works, the hydrogen is all assumed to be in H_2O, though it is almost certainly in hydroxyl (OH) instead. For this reason, we refer to it as "equivalent water content". However, the geological interpretation is the same whether the hydrogen is found in OH or H_2O; the hydrogen-bearing minerals were formed through aqueous alteration on the parent body (or perhaps through nebular processes which created phyllosilicates) and are now visible on the surface (see Zolensky *et al.*, 1997 for a recent discussion of meteoritical interpretations of water-bearing minerals). Other hydrogen carriers such as organic carbon compounds are not likely to be found in amounts comparable to clays on asteroid surfaces. If an asteroidal surface is very organic-rich, but OH-poor, it would appear to have a low H/Si ratio by this technique. However, such an asteroid spectrum would look quite different from the ones presented here, and would certainly be flagged for further study. Searches for organic materials on asteroids in this spectral region have so far yielded negative results (Cruikshank *et al.*, 2002; Emery, 2002).

We used a bulk SiO_2 concentration of 30%, which is the CM average reported in Jarosewich. Given this, we can determine the equivalent water content of the target asteroids from their reflectance spectra:

$$\text{Equiv. Water} = 0.5 \times \text{H/Si} \times \text{wt. frac. SiO}_2 \times \frac{\text{atomic wt. H}_2\text{O}}{\text{atomic wt. SiO}_2} \qquad (3)$$

The factor of 0.5 is necessary to account for the fact that two hydrogens go into water, rather than just one. This is why the explicit assumption that the hydrogen is in water rather than hydroxyl is necessary. The calculated water contents for the target asteroids are shown in Figure 9. The equivalent water contents for the asteroids are shown using the 2.9-μm reflectance ratio only. An estimate of the uncertainties involved in the calculations is provided below, in Section 4.4.

Because the H/Si ratio does not contain any assumptions about the silicate mineralogy of the target asteroids, it is preferred for quantitatively determining good analogs. However, the water contents are also included here since they potentially provide a good qualitative means of comparison with a wide range of materials, and because the weight fraction of water is a more familiar quantity than H/Si ratio.

4.4 Test on meteorites

We tested the accuracy of Equations 1–3 by determining the water contents for six meteorites for which we had both published 3-μm spectra and laboratory geochemical data. The calculated water content was determined from both the 2.9 and 3.2 μm reflectances and averaged, using the known SiO_2 concentration for each meteorite. Figure 7 shows the results. The measured water contents are derived from Hiroi *et al.* (2001) for Tagish Lake and Jarosewich (1990) for the other five meteorites. The line in Figure 7 represents where the points would lie if the calculated water contents were equal to the measured water contents. It is important to note that this is *not* a best-fit line. The average difference between the water values calculated from the meteorite spectra and the known water values, weighted by the uncertainties in the spectral data, is 1.0% $\pm$ 1.7%. The unweighted average difference is 1.0% $\pm$ 2.7%. If only the 2.9 μm reflectance is used to determine the water content, the mean difference is smaller, though with larger uncertainties: 0.064% $\pm$ 2.2% (unweighted) or 0.33% $\pm$ 2.5% (weighted).

It is worth noting that all of these meteorites except for Tagish Lake were used by Sato *et al.* (1997) in finding the original correlations in their work. However, the spectra used in our test are from a different source, Hiroi *et al.* (1996). We also note that the reflectance ratios in this work use 2.50 μm rather than 2.53 μm as used by Sato *et al.*, 1997. This is because 2.53 μm is a somewhat more difficult wavelength to observe from the ground. Because the reflectances of the target objects should not be changing appreciably between 2.50 and 2.53 μm, we expect the uncertainties introduced by this change to be negligible. Indeed, the fact that the meteorite data matches the known water values so closely is evidence of this.

We also include in Figure 7 the results if we assume the meteorites have a weight percentage of 30% SiO_2, as we do with the asteroids. As can be seen, for most of the meteorites the change is relatively small but for Orguiel, which has a large amount of water but a small bulk SiO_2 content, the effect is relatively large.

4.5 Results for asteroids

The H/Si ratios calculated for the asteroids using both the 2.9-μm and 3.2-μm ratios is shown in Figure 8. Although the H/Si values derived from the 3.2-μm data are shown, the 2.9-μm-derived values are the only ones discussed below. This is because uncertainties in thermal corrections lead to additional uncertainties in H/Si ratio of roughly 0.5 in the 3.2-μm-derived data, which are not reflected in the figure. These same uncertainties only amount to $\sim$0.1 or less in the 2.9-μm-derived H/Si values. The meteorite zones are based on data from falls in Jarosewich (1990), with estimated bounds. The asteroids fall into two main groups, with the first group perhaps really representing two sub-groups:

1. a H/Si > 2 (51 Nemausa, 13 Egeria, 106 Dione): These asteroids have H/Si ratios similar to or slightly greater than the CM meteorites.

2. b H/Si ~ 1.6 (5 asteroids): This H/Si ratio is roughly 2/3 that of the CM value. This group may be combined with the first group.

3. H/Si < 0.8 (8 asteroids): This group includes both asteroids which are anhydrous within uncertainties and those which have a small amount of hydrated minerals. The CV and CO chondrites have similar amounts (or lack of) hydrated minerals, but these values are not diagnostic for these meteorite groups; metamorphosed carbonaceous chondrites of other groups also contain little or no hydrated minerals.

Figure 8 also shows the averages for different Bus classes. Taken as a whole, the Ch asteroids have H/Si ratios consistent with CM meteorites. The C and B classes have ratios which are much lower, particularly if Ceres and Pallas are excluded. Ceres is an unusual asteroid in terms of its 3-μm spectrum, and its exclusion from the C asteroid average is justifiable on those grounds. Excluding Pallas from the B asteroid average is more arbitrary. At this point with only three B asteroids surveyed, it is unclear whether Pallas is truly unusual compared to its classmates or whether the B class spans a wide range of H/Si ratios.

5 Discussion

5.1 Ceres and Ursula

Figure 10 shows the spectra of 1 Ceres and 375 Ursula (with a linear continuum removed), the two asteroids in this sample which do not follow the carbonaceous chondrite trend in Figure 4. To this point, it was thought that Ceres was unique among low-albedo asteroids in its unusual band shape. The interpretation of this shape as being due to ammoniated silicates by King *et al.* (1992) suggests aqueous alteration by a fluid containing NH_4^+ and constrains the temperatures experienced by Ceres' surface to 400K or less (Lewis and Prinn, 1984; Chourabi and Fripiat, 1981). Ceres' current maximum surface temperature is $\sim$235 K (Tedesco *et al.*, 1992; Saint-Pe *et al.*, 1993) The alternate interpretation for Ceres' surface, that of water frosts, is only possible at very high latitudes at Ceres' surface temperatures (Fanale and Salvail, 1989).

The spectrum of 375 Ursula is similar to that of Ceres, though the wavelengths of band minima are not identical. Ursula is farther from the Sun, though its lower albedo compared to Ceres will raise its temperature. These competing effects result in a surface temperature only $\sim$10 K lower than Ceres. This difference in temperature is unlikely to make water ice stable over large portions of Ursula's surface. A low-temperature ammoniated phyllosilicate interpretation is preferred for this reason, though this may not be the only possibility. Higher-albedo asteroids with 3-μm features (*e.g.* 44 Nysa, 92 Undina, 21 Lutetia) have been found to have rounded bands that are at least superficially like those on Ceres and Ursula. We note that Ursula is classified as Xc in the Bus taxonomy, which is the same class as 44 Nysa, though the albedos are vastly different for these two asteroids (0.032 for Ursula, 0.546 for Nysa: Millis *et al.*, 1984; Tedesco *et al.*, 1992). It is unclear at this point how common low-albedo asteroids with rounded 3-μm bands are, though it seems unlikely that Ceres and Ursula are the only two.

5.2 G-class Asteroids

In the Tholen (1984) taxonomy, the G class is a subclass related to the C, F, and B classes. The Bus and Binzel (2002) taxonomy does not include a G class. Vilas (1994) found the G-class asteroids to be the most hydrated of the CBGF clan, based on the presence on most of these asteroids of the 0.7-μm band correlated with hydrated minerals. Burbine (1998) proposed that the G-class asteroids were analogs for the CM chondrites based upon their 0.3–2.5 μm spectra (particularly their 0.7-μm band), as well as dynamical arguments. Four of the asteroids in our sample are G asteroids: 1 Ceres, 13 Egeria, 19 Fortuna, and 106 Dione. Ceres is unusual for several reasons, as mentioned above, and can be discounted. Interestingly, Egeria and Dione are two of the three asteroids with water contents consistent with the CM average within observational uncertainties, and Fortuna is also in the high-water group. This supports the hypothesis of Burbine.

5.3 Where are the CI parents?

The lack of parent bodies with CI-like H/Si ratios is striking. One possibility is that our sample size is still relatively small, and we have not come across any CI parent bodies yet. Related to that is the possibility that they are not very common in the asteroid belt, and so we will need to observe many more objects before finding one. A third possibility is that CI material is found mixed with less-hydrated or anhydrous material on the surface of its parent body(ies), lowering the apparent H/Si ratio to CM levels or below. Given the pervasiveness of aqueous alteration in CI meteorites, however, combined with their brecciated nature, we do not suspect this is the case. It is also conceivable that regolith processes have dehydrated CI surfaces to appear more like CM-like surfaces in terms of H/Si ratio. We discuss this below. Finally, given the fragility of CI material, it is possible that the CI meteorites come from objects too small (and thus too faint) to be observed at 3-μm with current telescopes and instruments. Given these options, we believe the likeliest is a combination of the first, second, and last: that CI material is relatively rare at large asteroidal sizes and that our sample size is too small to be certain of seeing one.

5.4 Space Weathering

There are two ways that regolith processes could plausibly change the 3-μm spectra of hydrated bodies. First, vapor-deposited nanophase iron (npFe) could alter spectral properties of surfaces without necessarily changing their compositions. This process, often called "space weathering", is observed in the visible and near-IR spectra of lunar soils and is also thought to be present in the visible and near-IR spectra of S asteroids (Sasaki *et al.*, 2001; Pieters *et al.*, 2000). The effect lessens as wavelength increases, and in low-albedo ($p_v \lesssim 0.1$) objects, which suggests that this will not be an important concern here. We note that experiments on npFe deposition in carbonaceous chondrites are currently underway.

A second possibility is that impacts into the surface of a hydrated asteroid could devolatilize and dehydrate the regolith. This would presumably lead to a surface with little or no obvious 3-μm band covering a hydrated interior. In this case, 3-μm observations would only provide a lower limit to band depth and a lower limit to water content, though the observations would accurately depict the surface mineralogy.

The observations presented here directly touch upon the question of spectral alteration in the 3-μm region, and allow us to quantitatively estimate the relative rate at which any putative dehydration may occur. If dehydration were to occur quickly relative to regolith turnover timescales, we would expect most of the asteroids to have H/Si ratios near zero, with only rare instances of H/Si values higher than that. This is not the case in our sample. If dehydration were occurring on the same timescale as regolith turnover, we would expect to see objects throughout the range of H/Si ratios, with perhaps more in the middle. This is arguably the case here, though our sample size is too small to make a strong case either way. Finally, if dehydration is very slow relative to regolith turnover, we would expect objects to remain near their bulk H/Si values. Again, this is arguably the case here. The CM-like H/Si ratios for the G-class asteroids suggests that the proposed G-CM link can be interpreted with no need to consider regolith effects, and that dehydration is not important at least for that group.

Hiroi *et al.* (1996) suggested that large C-class (and the related B, G, and F-class) asteroids were thermally metamorphosed early in solar system history, based on the relative strengths of their 0.7-μm and 3-μm bands. The data presented here do not explicitly address these findings, but do provide an additional 11 asteroids with which to test their model. We recalculated the 0.7-μm band depth for 14 of our target asteroids using the ECAS data of Zellner *et al.* (1985) and the formula included in Vilas (1994), and compared it to the 2.9-μm band depth in Table 3. This is shown in Figure 11. The asteroids 324 Bamberga and 375 Ursula do not have ECAS data at the necessary wavelengths, and so were omitted. Figure 11 shows an good correlation between the two band depths, although it is not a perfect one. This is consistent with the idea that thermal effects may have destroyed phyllosilicates and weakened the 3-μm and 0.7-μm bands in tandem. However, this is not a unique interpretation and a number of large asteroids like 2 Pallas with a strong 3-μm band but little or no 0.7-μ absorption need an alternate explanation.

6 Future Work

At this point, reflectances at 2.5, 2.9, and 3.2 μm are necessary to determine H/Si ratios for C-class asteroids directly from reflectance spectra using the relations outlined above. The majority of asteroid data thus far collected for these objects in the 3-μm region is spectrophotometric rather than spectroscopic, however (Lebofsky, 1980; Feierberg *et al.*, 1985; Britt *et al.*, 1994), and reflectances at 2.9 and 3.2 μm are not available. However, because the 3-μm band for most hydrated asteroids has a simple, linear slope through 2.9 and 3.2 μm out to the continuum, it should be possible to recalculate Equations 1 and 2 for other wavelengths inside the 3-μm band. This would dramatically increase our sample size of usable data.

The discovery of a 3-μm band on M-, S-, and E-class asteroids (Jones *et al.*, 1990; Rivkin *et al.*, 1995; Rivkin *et al.*, 2000; Rivkin *et al.*, 2001) potentially allows remote determination of H/Si for these bodies as well. However, their higher albedos makes it uncertain whether carbonaceous chondrite powders are sufficiently analogous to their surfaces. Clark (1983) showed that the

3-μm band in montmorillonite decreased in depth with increasing amounts of carbon mixed in. With over 90% of the spectrally opaque carbon mixed in, the 3-μm band decreased in strength by 50%. As an initial guess, we might be able to simply divide the band depths by two on these high-albedo objects to simulate mixing in 90% opaques and creating a carbonaceous-chondrite-like albedo. An actual analysis of this technique would obviously need to be done before the H/Si values generated would be of use.

7 Conclusions

We have observed sixteen low-albedo objects in the 3-μm region from UKIRT from 1996-2000. Using relations first derived for meteorites by Miyamoto and Zolensky (1994) and Sato *et al.* (1997), we have determined the hydrogen to silicon ratios for these bodies, which divide into two groups. Some of the targets are consistent with CM meteorite values for H/Si, but none are consistent with CI meteorites. We believe this suggests that CI parent bodies are relatively uncommon. We found 375 Ursula to have a 3-μm band shape reminiscent of 1 Ceres, suggesting that the former asteroid may have a surface containing ammoniated silicates, as has been proposed for Ceres.

Band depths at 3 μm and 0.7 μm appear correlated, though individual objects may vary. Future work includes adapting the H/Si relations to allow for archival data to be analyzed and attempting to expand our analysis to asteroids of other types than carbonaceous-chondrite-like asteroids.

Acknowledgments: This work was supported by NASA grants NAG5-10604 and NAG5-11617. The United Kingdom Infrared Telescope is operated by the Joint Astronomy Centre on behalf of the U.K. Particle Physics and Astronomy Council. Mahalo nui loa to the telescope operators at UKIRT and the support crew on Mauna Kea. The majority of the observing and much of the work in this paper was conducted by ASR while he was at the University of Arizona. We also extend our gratitude to the people of Hawaiian descent, who have allowed us to visit their sacred mountain of Mauna Kea to conduct our research.

*References

Britt, D. T., A. S. Rivkin, E. S. Howell, and L. A. Lebofsky (1994). Observations of "dry" C class asteroids. *Bull. Amer. Astr. Soc.* **26**, 1175.

Burbine, T. H. (1998). Could G-class asteroids be the parent bodies of the CM chondrites? *Meteoritics and Planetary Science* **33**, 253–258.

Burbine, T. H., M. J. Gaffey, and J. F. Bell (1992). S-asteroids 387 Aquitania and 908 Anacostia: Possible fragments of the breakup of a spinel-bearing parent body with CO3/CV3 affinities. *Meteoritics* **27**, 424–434.

Bus, S. J. and R. P. Binzel (2002). Phase II of the Small Main-Belt Asteroid Spectroscopic Survey: A Feature-Based Taxonomy. *Icarus* **158**, 146–177.

Chourabi, B. and J. J. Fripiat (1981). Determination of tetrahedral substitutions and interlayer surface heterogeneity from vibrational spectra of ammonium in smectites. *Clays Clay Minerals* **29**, 260–268.

Clark, R. N. (1983). Spectral properties of mixtures of montmorillonite and dark carbon grains: Implications for remote sensing minerals containing chemically and physically adsorbed water. *J. Geophys. Res.* **88**, 10635–10644.

Cruikshank, D. P., T. R. Geballe, T. C. Owen, C. M. Dalle Ore, T. L. Roush, R. H. Brown, and J. H. Lewis (2002). Search for the 3.4-μm

C-H Spectral Bands on Low-Albedo Asteroids. *Icarus* **156**, 434–441.

Delsemme, A. H. (2000). 1999 kuiper prize lecture. *Icarus* **146**, 313–325.

DuFresne, E. R. and E. Anders (1962). On the chemical evolution of the carbonaceous chondrites. *Geochim. Cosmochim. Acta* **26**, 1084–1114.

Emery, J. P. (2002). *Constraints on the surface composition of Trojan asteroids from near infrared (0.8–4.0 μm) spectroscopy and spectral modeling*. Ph.D. dissertation, University of Arizona, Tucson, AZ.

Fanale, F. P. and J. R. Salvail (1989). The water regime of asteroid (1) Ceres. *Icarus* **82**, 97–110.

Feierberg, M. A., L. A. Lebofsky, and D. Tholen (1985). The nature of C-class asteroids from 3-μm spectrophotometry. *Icarus* **63**, 183–191.

Gaffey, M. J., J. F. Bell, and D. P. Cruikshank (1989). Reflectance spectroscopy and asteroid surface mineralogy. In R. Binzel, T. Gehrels, and M. S. Matthews (Eds.), *Asteroids II*, pp. 98–127. Tucson: University of Arizona Press.

Harris, A. W. (1998). A Thermal Model for Near-Earth Asteroids. *Icarus* **131**, 291–301.

Hiroi, T., M. E. Zolensky, and C. M. Pieters (2001). The Tagish Lake meteorite: A possible sample for a D-type asteroid. *Science* **293**, 2234–2236.

Hiroi, T., M. E. Zolensky, C. M. Pieters, and M. E. Lipschutz (1996). Thermal metamorphism of the C, G, B, and F asteroids seen from the 0.7 μm, 3 μm and UV absorption strengths in comparison with carbonaceous chondrites. *Meteoritics and Planetary Science* **31**, 321–327.

Hörz, F., R. Grieve, G. Heiken, P. Spudis, and A. Binder (1991). Lunar surface processes. In G. H. Heiken, D. T. Vaniman, and B. M. French (Eds.), *Lunar Sourcebook : A User's Guide to the Moon*, pp. 61–120. Cambridge: Cambridge University Press.

Howell, E. S., A. S. Rivkin, and F. Vilas (2001). Uneven distribution of aqueously altered minerals on asteroids. In *Asteroids 2001: from Piazzi to the third millenium*, pp. 62.

Jarosewich, E. (1990). Chemical analyses of meteorites: A compilation of stony and iron meteorite analyses. *Meteoritics* **25**, 323–337.

Jones, T. D., L. A. Lebofsky, J. S. Lewis, and M. S. Marley (1990). The composition and origin of the C, P, and D asteroids: Water as a tracer of thermal evolution in the outer belt. *Icarus* **88**, 172–192.

King, T. V. V., R. N. Clark, W. M. Calvin, D. M. Sherman, and R. H. Brown (1992). Evidence for ammonium-bearing minerals on Ceres. *Science* **255**, 1551–1553.

Koornneef, J. (1983). Near-infrared photometry. ii- intrinsic colours and absolute calibration from one to five microns. *Astron. Astrophys.* **128**, 84–93.

Larson, H. P., M. A. Feierberg, and L. A. Lebofsky (1983). The composition of 2 Pallas and its relation to primitive meteorites. *Icarus* **56**, 398–408.

Lebofsky, L. A. (1978). Asteroid 1 Ceres: Evidence for water of hydration. *MNRAS* **182**, 17–21.

Lebofsky, L. A. (1980). Infrared reflectance spectra of asteroids: A search for water of hydration. *Astron. J.* **85**, 573–585.

Lebofsky, L. A., M. A. Feierberg, A. T. Tokunaga, H. P. Larson, and J. R. Johnson (1981). The 1.7- to 4.2-micron spectrum of asteroid 1 Ceres: Evidence for structural water in clay minerals. *Icarus* **48**, 453–459.

Lebofsky, L. A. and J. R. Spencer (1989). Radiometry and thermal modeling of asteroids. In R. Binzel, T. Gehrels, and M. S. Matthews (Eds.), *Asteroids II*, pp. 128–147. Tucson: University of Arizona Press.

Lebofsky, L. A., M. V. Sykes, E. F. Tedesco, G. J. Veeder, D. L. Matson, R. H. Brown, J. C. Gradie, M. A. Feierberg, and R. J. Rudy (1986). A refined "standard" thermal model for asteroids based on observations of 1 Ceres and 2 Pallas. *Icarus* **68**, 239–251.

Lewis, J. S., D. S. McKay, and B. C. Clark (1993). Using resources from near-Earth space. In J. S. Lewis, M. S. Matthews, and M. L. Guerrieri (Eds.), *Resources of Near-Earth Space*, pp. 3–14. Tucson: University of Arizona Press.

Lewis, J. S. and R. G. Prinn (1984). *Planets and Their Atmospheres; Origin and Evolution*. Orlando: Academic Press, Inc.

Millis, R. L., L. H. Wasserman, E. Bowell, O. G. Franz, A. Klemola, and D. W. Dunham (1984). The diameter of 375 URSULA from its occultation of AG + 39^{o} 303. *Astron. J.* **89**, 592–596.

Miyamoto, M. and M. E. Zolensky (1994). Infrared diffuse reflectance spectra of carbonaceous chondrites: Amount of hydrous minerals. *Meteoritics* **29**, 849–853.

Morbidelli, A., J. Chambers, J. I. Lunine, J. M. Petit, F. Robert, G. B. Valsecchi, and K. E. Cyr (2000). Source regions and time scales for the delivery of water to Earth. *Meteoritics and Planetary Science* **35**, 1309–1320.

Mountain, C. M., D. J. Robertson, T. J. Lee, and R. Wade (1990). An advanced cooled grating spectrometer for UKIRT. In *Instrumentation in astronomy VII; Proceedings of the Meeting, Tucson, AZ, Feb. 13-17, 1990 (A91-29601 11-35). Bellingham, WA, Society of Photo-Optical Instrumentation Engineers, 1990.*, pp. 25–33.

Pieters, C. ., L. A. Taylor, S. K. Noble, L. P. Keller, B. Hapke, R. V.

Morris, C. C. Allen, D. S. McKay, and S. Wentworth (2000). Space weathering on airless bodies: Resolving a mystery with lunar samples. *Meteoritics and Planetary Science* **35**, 1101–1107.

Rivkin, A. S., J. K. Davies, B. E. Clark, D. E. Trilling, and R. H. Brown (2001). Aqueous Alteration on S Asteroid 6 Hebe? In *Lunar and Planetary Science Conference*, Volume 32, pp. abst. no. 1723.

Rivkin, A. S., E. S. Howell, D. T. Britt, L. A. Lebofsky, M. C. Nolan, and D. D. Branston (1995). 3-μm spectrophotometric survey of M and E-class asteroids. *Icarus* **117**, 90–100.

Rivkin, A. S., L. A. Lebofsky, B. E. Clark, E. S. Howell, and D. T. Britt (2000). The nature of M-class asteroids in the 3-μm region. *Icarus* **145**, 351–368.

Saint-Pe, O., M. Combes, and F. Rigaut (1993). Ceres surface properties by high-resolution imaging from earth. *Icarus* **105**, 271–281.

Salisbury, J. W., L. S. Walter, N. Vergo, and D. M. D'Aria (1991). *Infrared (2.1–25 μm) Spectra of Minerals.* Baltimore: Johns Hopkins University Press.

Sasaki, S., K. Nakamura, Y. Hamabe, E. Kurahashi, and T. Hiroi (2001). Production of iron nanoparticles by laser irradiation in a simulation of lunar-like space weathering. *Nature* **410**, 555–557.

Sato, K., M. Miyamoto, and M. E. Zolensky (1997). Absorption bands near three micrometers in diffuse reflectance spectra of carbonaceous chondrites: Comparison with asteroids. *Meteoritics and Planetary Science* **32**, 503–507.

Storrs, A., B. Weiss, B. Zellner, W. Burleson, R. Sichitiu, E. Wells, C. Kowal, and D. Tholen (1999). Imaging Observations of Asteroids with Hubble Space Telescope. *Icarus* **137**, 260–268.

Tedesco, E. F., G. J. Veeder, J. W. Fowler, and J. R. Chillemi (1992). *The IRAS Minor Planet Survey Data Base.* Greenbelt, Maryland: National Space Science Data Center. digital data.

Tholen, D. J. (1984). *Asteroid taxonomy from cluster analysis of photometry.* Ph.D. dissertation, University of Arizona, Tucson, AZ.

Vilas, F. (1994). A cheaper, faster, better way to detect water of hydration on solar system bodies. *Icarus* **111**, 456–467.

Zellner, B., D. J. Tholen, and E. F. Tedesco (1985). The eight-color asteroid survey: Results for 589 minor planets. *Icarus* **61**, 355–416.

Zolensky, M. E., A. N. Krot, and E. R. D. Scott (Eds.) (1997). *Workshop on Parent-Body and Nebular Modifications of Chondritic Materials.* Houston: Lunar and Planetary Institute. LPI Tech. Rpt. 97-02, Part 1.

Date	Asteroid	Tholen	Bus	Standard	Observers
4 Feb 1996	2 Pallas	B	B	BS 5384	Rivkin, Davies,
	13 Egeria	G	Ch	BS 1164	Johnson
	51 Nemausa	CU	Ch	SAO 11691	
10 Jul 1997	1 Ceres	G	C	SAO 165572	Rivkin, Davies,
	19 Fortuna	G	Ch	SAO 146142	Ellison
	106 Dione	G	Cgh	SAO 188048	
11 Aug 1998	185 Eunike	C	C	BS 9107	Rivkin, Davies
	375 Ursula	C	Xc	BS 9107	
12 Aug 1998	980 Anacostia	SU	L	BS 6836	
	521 Brixia	C	Ch	BS 88	
13 Aug 1998	59 Elpis	CP	B	BS 6998	
	238 Hypatia	C	Ch	BS 8314	
28 Jan 2000	45 Eugenia	FC	C	BS 4533	Rivkin, Davies, Trilling
29 Jan 2000	52 Europa	CF	C	SAO 119398	
2 Oct 2000	324 Bamberga	CP	-	SAO 56391	Rivkin, Davies
4 Oct 2000	704 Interamnia	F	B	SAO 161071	

Table 1: Asteroids Observed at UKIRT. Taxonomic classifications in both the Bus and Binzel and Tholen schemes are included, as well as the observers present at the telescope.

Asteroid	Diameter	Albedo	η
1 Ceres	848 km	0.113	0.756
2 Pallas	498 km	0.159	0.756
13 Egeria	208 km	0.083	0.90
19 Fortuna	225 km*	0.05*	0.90
45 Eugenia	215 km	0.040	0.90
51 Nemausa	148 km	0.093	0.90
52 Europa	303 km	0.058	0.85
59 Elpis	165 km	0.044	0.85
106 Dione	147 km	0.089	0.85
185 Eunike	158 km	0.064	0.85
238 Hypatia	149 km	0.043	1.00
324 Bamberga	229 km	0.063	0.78
375 Ursula	216 km*	0.032*	0.90
521 Brixia	116 km	0.063	0.756
704 Interamnia	317 km	0.074	0.85
980 Anacostia	86 km	0.172	1.00

Table 2: The diameters, albedos, and thermal parameters (η) used in the thermal models for target asteroids. The diameters and albedos are from IRAS measurements, except for 19 Fortuna and 375 Ursula. The diameter of 19 Fortuna was taken from HST observations by Storrs et al. (1999), with its albedo derived from that diameter and its published absolute magnitude. Millis et al. (1984) found a the diameter of 375 Ursula from an occultation, and derived its albedo.

Asteroid	2.9-μm Band Depth	$\pm$	3.2-μm Band Depth	$\pm$
1 Ceres	20.4%	1.3%	19.0%	3.3%
2 Pallas	21.8	1.6	7.2	1.5
13 Egeria	30.3	2.6	12.6	4.8
19 Fortuna	23.8	2.2	7.5	5.4
45 Eugenia	0.4	2.6	-13.9	4.2
51 Nemausa	38.8	2.2	11.9	2.2
52 Europa	6.2	2.0	1.7	3.8
59 Elpis	-1.8	5.9	-5.1	5.9
106 Dione	40.2	8.4	19.6	29.6
185 Eunike	5.3	2.0	3.4	3.6
238 Hypatia	19.5	2.9	8.7	6.9
324 Bamberga	-1.9	2.0	-5.3	4.9
375 Ursula	3.6	1.8	4.2	3.3
521 Brixia	24.8	4.0	3.2	5.8
704 Interamnia	9.3	5.9	1.8	5.6
980 Anacostia	-0.2	4.4	0.6	2.5

Table 3: 2.9- and 3.2-μm band depths for target asteroids. These were calculated as(1 - $R_\lambda/R_{2.5\mu m}$), but have had modeled thermal flux removed. The 3.2-μm band depth is not near the band minimum, and is included to allow rederivation of H/Si ratios. The uncertainty for the band depths is the square root of the sum of the squares of the uncertainties at 2.5 μm and either 2.9 or 3.2 μm.

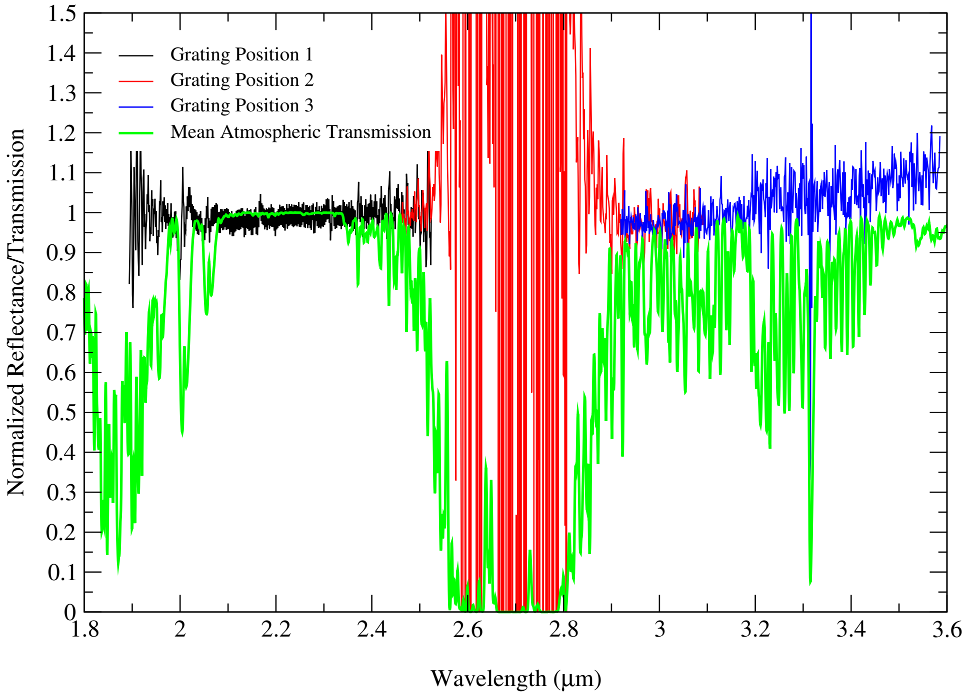

Figure 1: Grating positions and atmospheric transmission: The spectrum shown here (980 Anacostia/BS 6836) is composed of data taken in three grating positions, shown in black, red, and blue. The overlap enables us to create a single, continuous spectrum. Atmospheric transmission varies from 0–1 over the range of the spectrum.

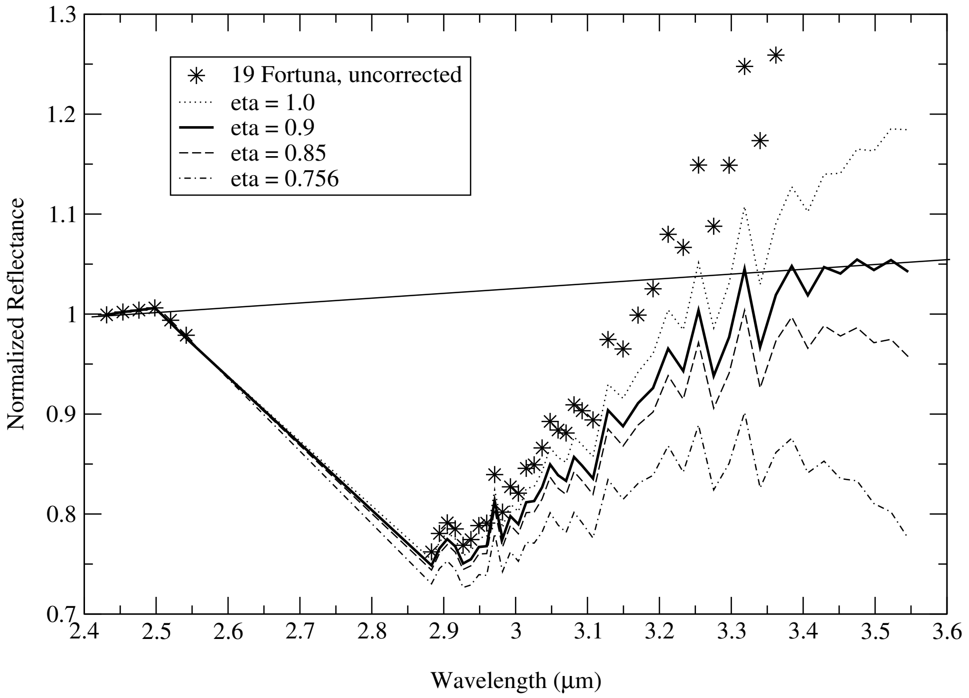

Figure 2: Effect of thermal corrections. Shown is the spectrum of 19 Fortuna, uncorrected (symbols) and corrected using thermal models with differing values of the beaming parameter (η). A value of η which is too small results in overcorrection of the data, and a spectrum which dips with increasing wavelength starting $\sim$3.4 μm. The model chosen (heavy solid line) results in a continuum near 3.5 μm of a similar slope to the continuum near 2.4 μm (light solid line).

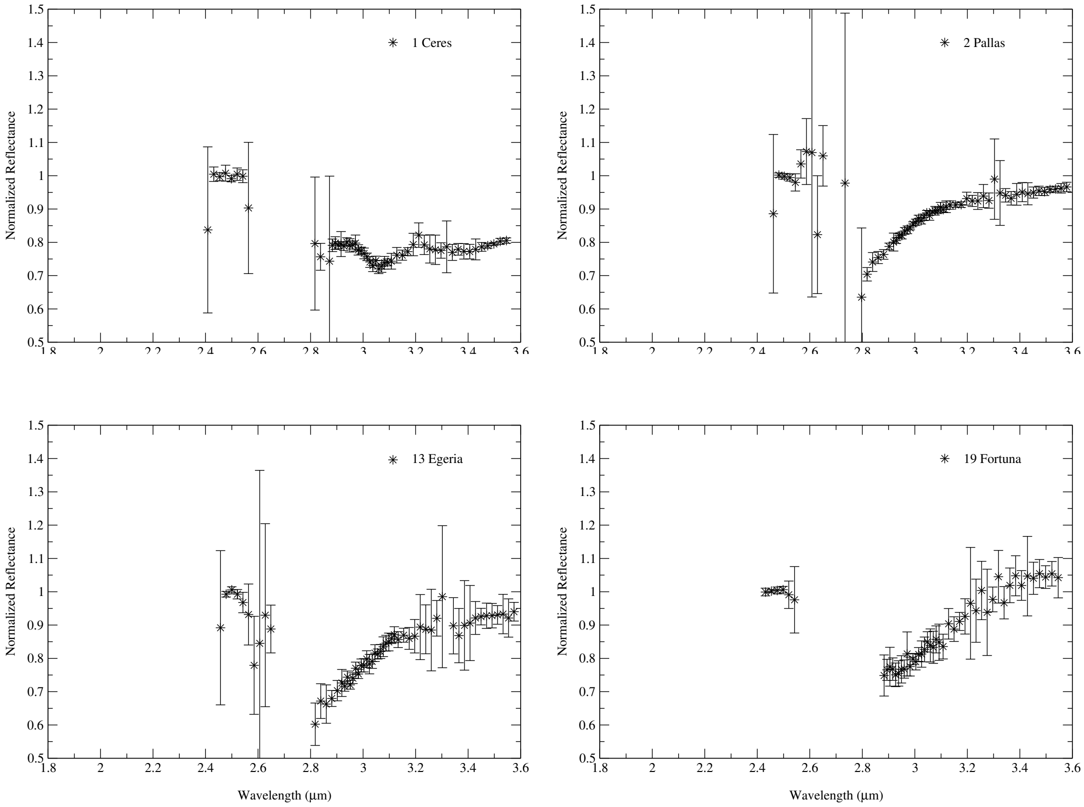
1 Ceres
2 Pallas
13 Egeria
19 Fortuna
Normalized Reflectance
Wavelength (μm)

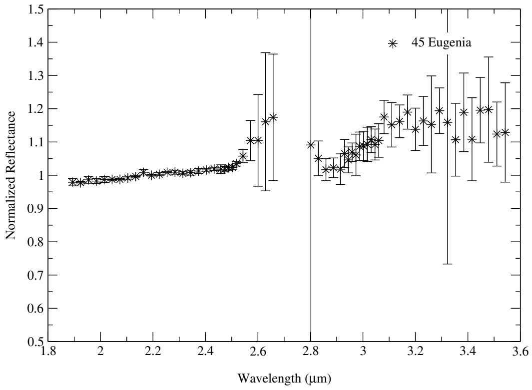
45 Eugenia
Normalized Reflectance
Wavelength (µm)
1.5
1.4
1.3
1.2
1.1
1
0.9
0.8
0.7
0.6
0.5
1.8
2
2.2
2.4
2.6
2.8
3
3.2
3.4
3.6

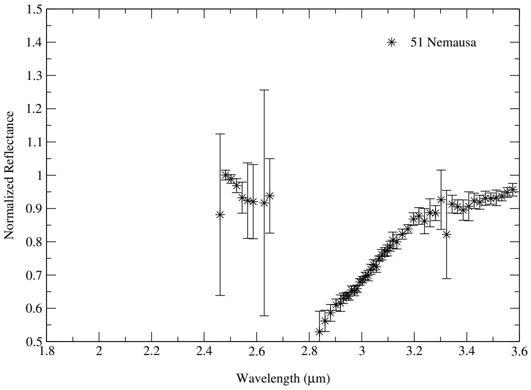
51 Nemausa
Normalized Reflectance
Wavelength (µm)
1.5
1.4
1.3
1.2
1.1
1
0.9
0.8
0.7
0.6
0.5
1.8
2
2.2
2.4
2.6
2.8
3
3.2
3.4
3.6

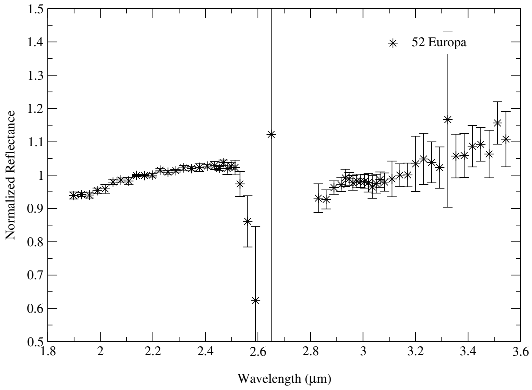
52 Europa
Normalized Reflectance
Wavelength (µm)
1.5
1.4
1.3
1.2
1.1
1
0.9
0.8
0.7
0.6
0.5
1.8
2
2.2
2.4
2.6
2.8
3
3.2
3.4
3.6

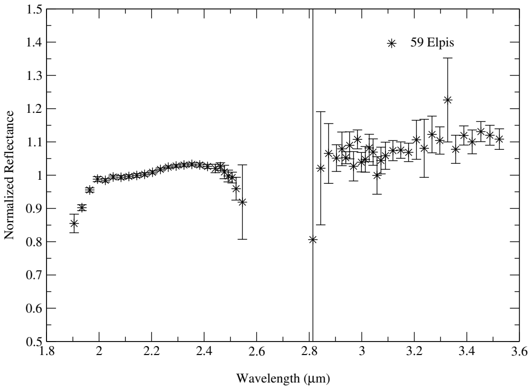
59 Elpis
Normalized Reflectance
Wavelength (µm)
1.5
1.4
1.3
1.2
1.1
1
0.9
0.8
0.7
0.6
0.5
1.8
2
2.2
2.4
2.6
2.8
3
3.2
3.4
3.6

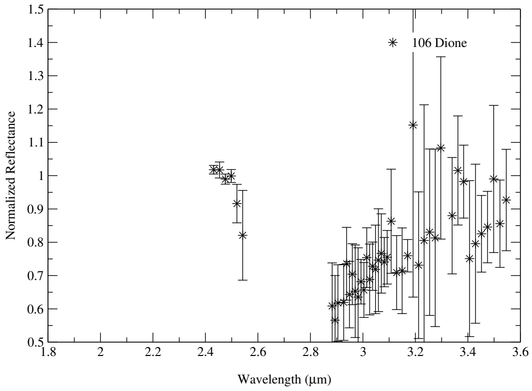
106 Dione
Normalized Reflectance
Wavelength (µm)
1.5
1.4
1.3
1.2
1.1
1
0.9
0.8
0.7
0.6
0.5
1.8
2
2.2
2.4
2.6
2.8
3
3.2
3.4
3.6

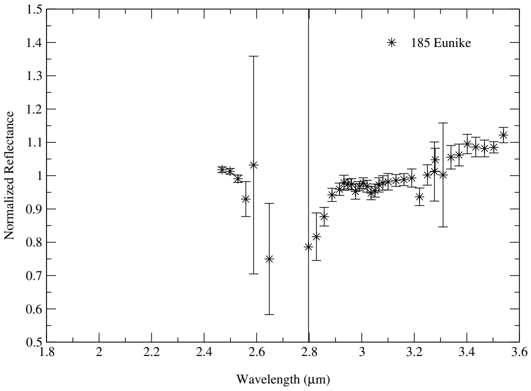
185 Eunike
Normalized Reflectance
Wavelength (µm)
1.5
1.4
1.3
1.2
1.1
1
0.9
0.8
0.7
0.6
0.5
1.8
2
2.2
2.4
2.6
2.8
3
3.2
3.4
3.6

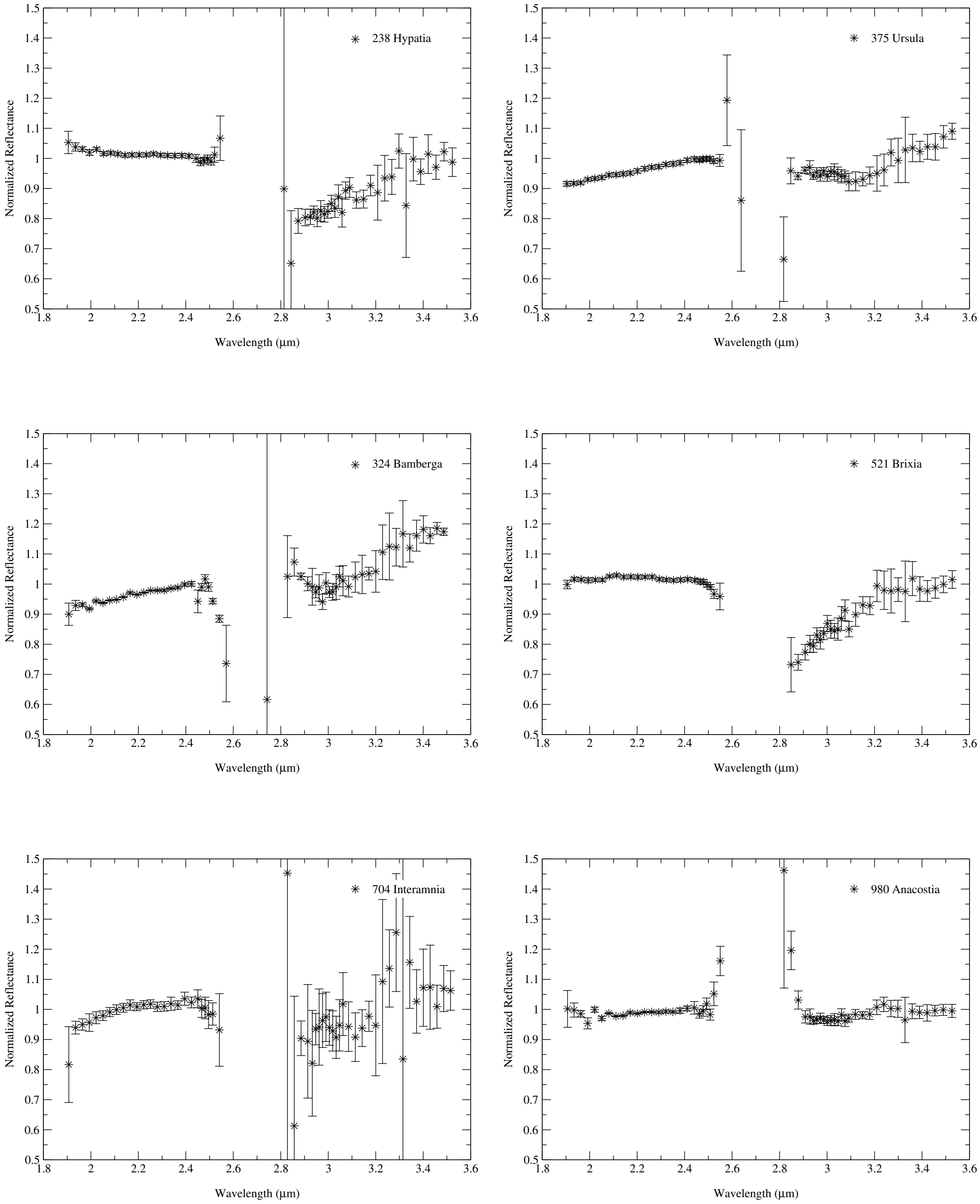

Figure 3: Thermally-corrected spectra of the target asteroids, 1996-2000.

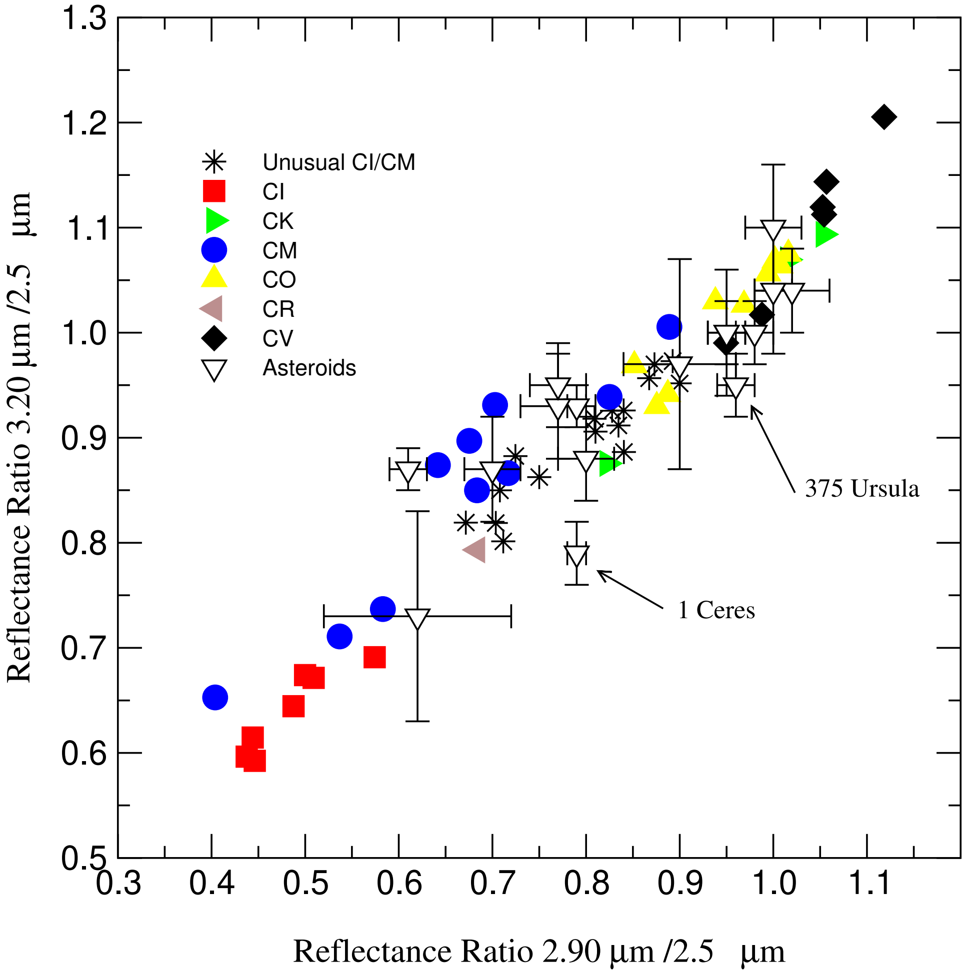

Figure 4: On a diagram of 3.2/2.5 μm reflectance vs. 2.9/2.5 μm reflectance, the carbonaceous chondrites follow a linear trend, first shown by Sato et al. (1997). The asteroids in this work also follow the same trend, except for 1 Ceres and 375 Ursula. Other than those two, the other asteroids all have spectra consistent with carbonaceous chondrites. The meteorite data in this plot are from Hiroi et al. (1996) and Jones (1988).

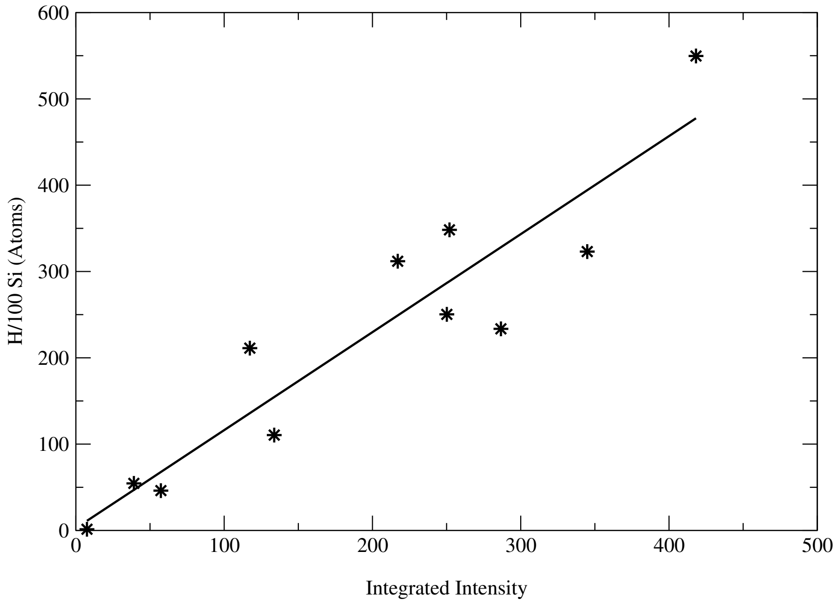

Figure 5: Correlation between the integrated intensity and H/Si ratio in carbonaceous chondrites. Using a digitized version of Figures 4 from Miyamoto and Zolensky (1994), we regenerated the linear correlation they reported for the integrated intensity of the 3-μm band for carbonaceous chondrite powders and their H/Si ratios and obtained the following relation: H/100 Si = $2.62935 + 1.13558 \times$ integrated intensity. The equation for this best-fit line was combined with the equation for the best-fit line in the following figure to give Equations 1 and 2. Integrated intensity is in units of cm^{-1}

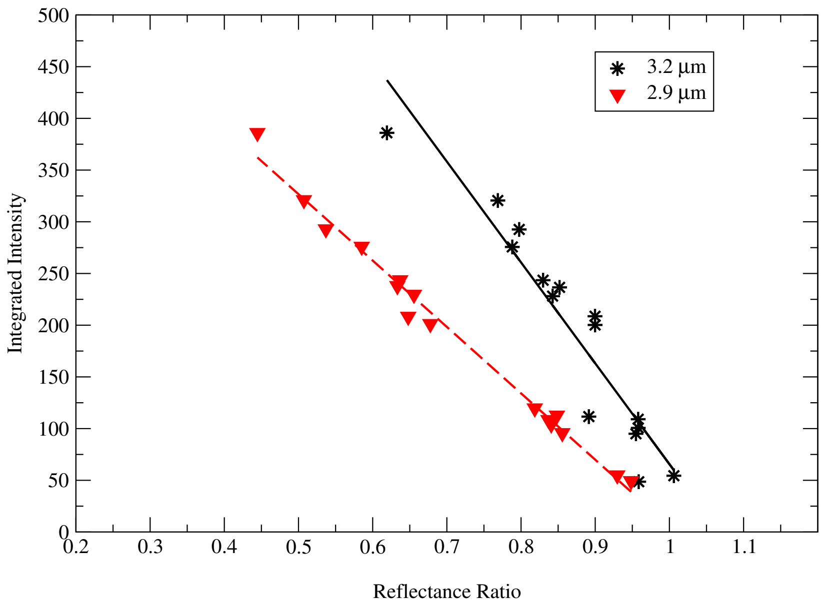

Figure 6: Correlation between reflectance ratios in the 3-μm region and integrated intensity in carbonaceous chondrites. Using digitized versions of Figure 3 from Sato et al. (1997), we regenerated the linear correlation they reported for 2.9-μm and 3.2-μm reflectance ratios, resulting in the following relations: integrated intensity = 647.63 - 641.90$\times\frac{R_{2.9}}{R_{2.53}}$ and integrated intensity = 1040.82 - 975.21$\times\frac{R_{3.2}}{R_{2.53}}$. The equations for these best fit lines were combined with the equation for the best-fit line in the previous figure to give Equations 1 and 2. Integrated intensity is in units of cm^{-1}

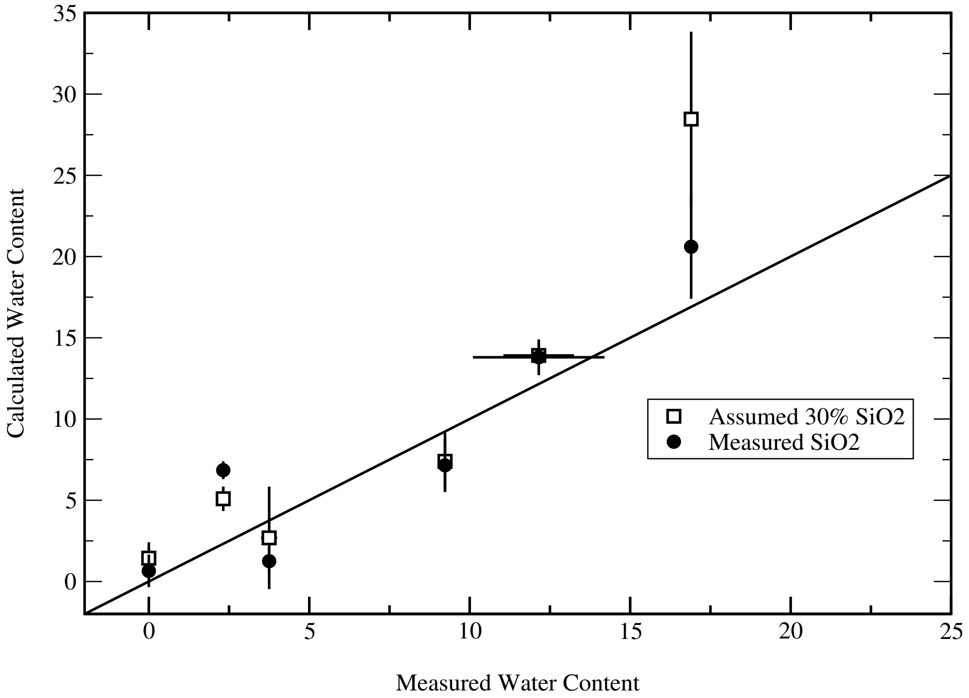

Figure 7: Using Equations 1 and 2 we determined the equivalent water content for six carbonaceous chondrites for which we have both geochemical data and reflectance spectra. The solid line is where predicted equals known values, and represents where the points should fall given perfect data and a perfect method. It is not a best fit line. The closed symbols use the known SiO_2 values from Jarosewich (199), the open symbols assume a SiO_2 concentration of 30%.

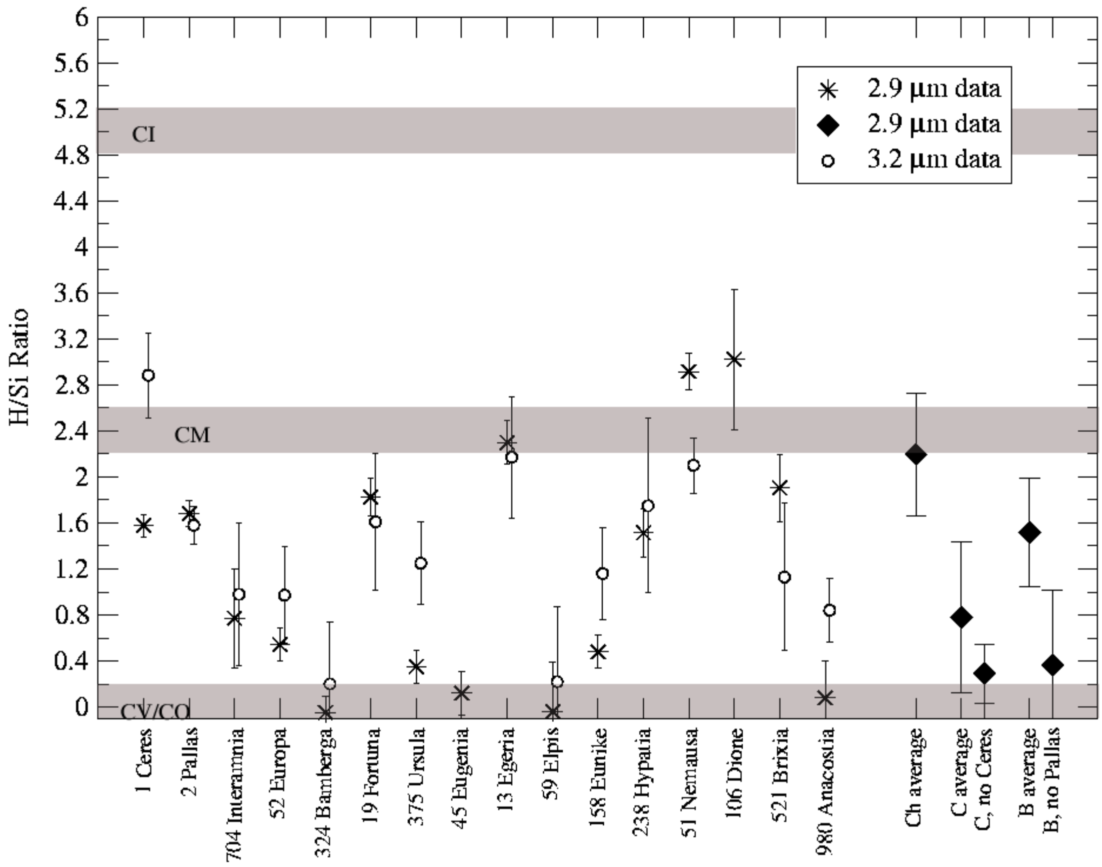

Figure 8: The calculated H/Si ratios for C-class and related asteroids (using Bus taxonomy). The Ch asteroids as a group have water contents consistent with the CM chondrites. The individual asteroids seem to form two groups, with the more hydrogen-rich group itself splitting into two groups. None of the target asteroids are consistent with CI H/Si ratios. These ratios were calculated using the 2.9-μm reflectance only, and the asteroids are in order of decreasing size..

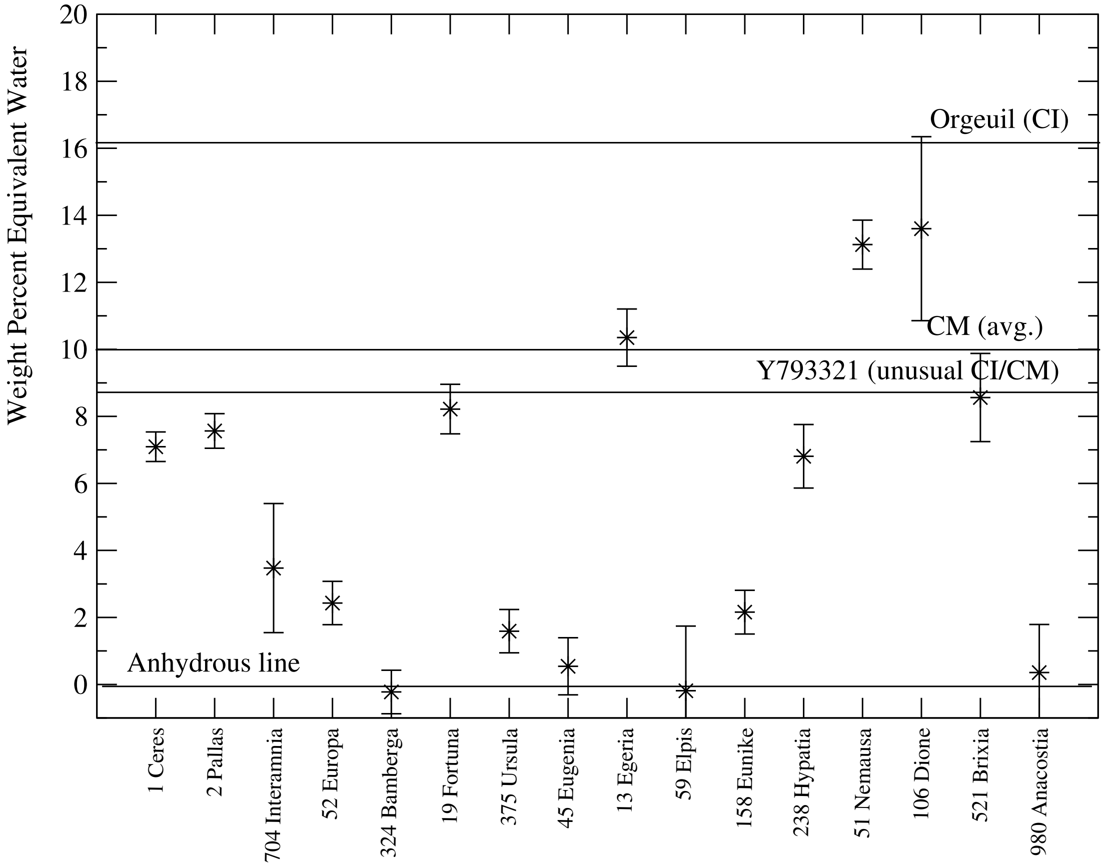

Figure 9: The calculated water contents for C-class and related asteroids. These values were calculated assuming a CM-like SiO2 weight percentage and using the H/Si ratio from the previous figure. Because the H/Si ratio is lower than CM values for most of these objects, the calculated water contents are also lower than CM values. On this figure, values for specific meteorites rather than shaded ranges are shown.

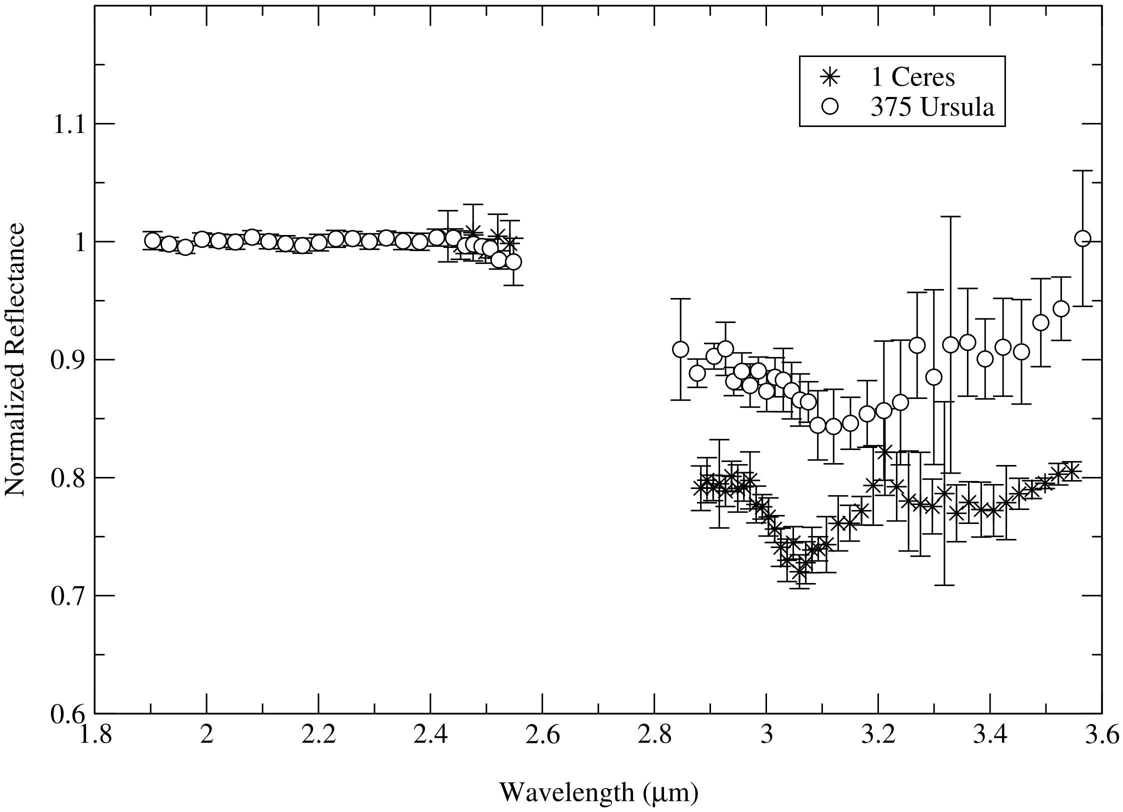

Figure 10: Spectra of 1 Ceres and 375 Ursula. These two objects fall off of the meteorite trend shown in Figure 5. Ceres is well-known to have an unusual band shape at 3 μm, and has a surface interpreted as either containing a water ice frost (Lebofsky 1981) or ammoniated phyllosilicates (King et al. 1992). The Ursula spectrum, shown with a linear continuum removed to facilitate comparison, shows a similar spectrum. This suggests that Ceres' surface mineralogy is not unique. It also favors the ammoniated phyllosilicate interpretation since water frost was only marginally stable on Ceres (Fanale and Salvail 1989).

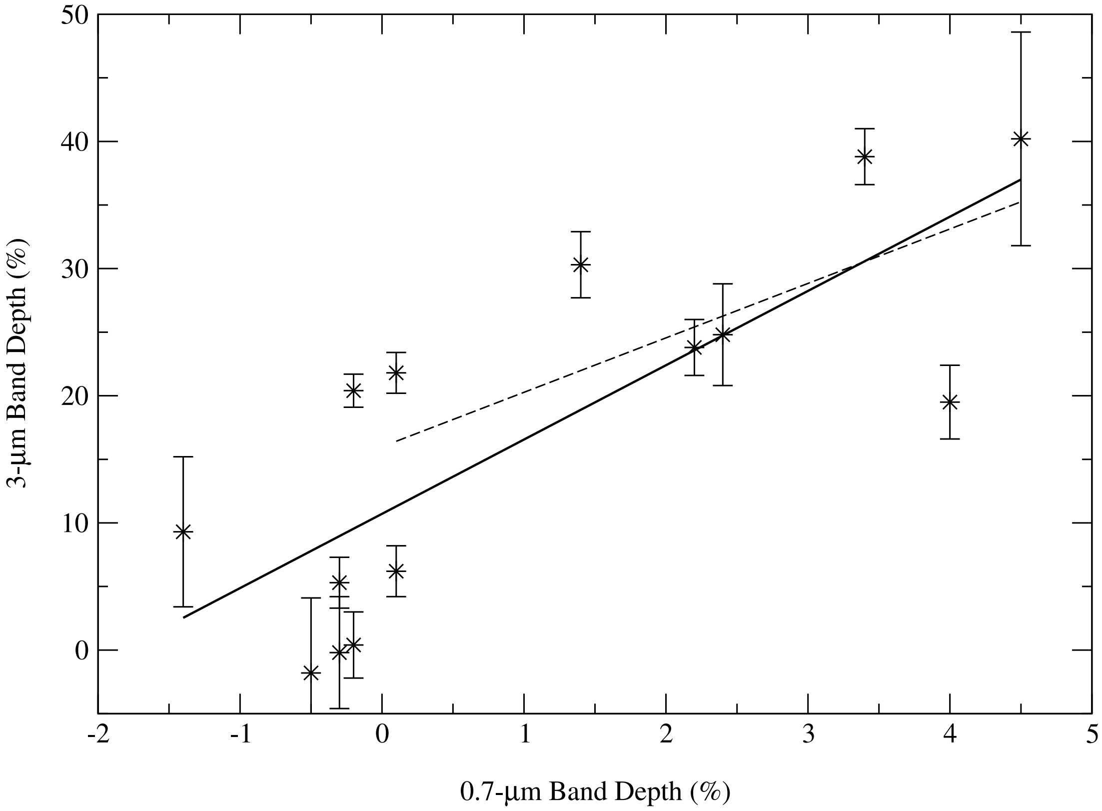

Figure 11: Correlation between the 0.7-μm band and the 3-μm band depths. The 0.7-μm band depth was determined using ECAS data (Zellner 1985)and the test of Vilas (1994), the 3-μm band depths from this work. The solid line shows the best-fit line including all of the points, the dashed line includes only points which have positive values for band depth. There is an obvious correlation between these two values in both cases, with a correlation coefficient of 0.783 when all of the points are included, and 0.651 with the smaller set of points.

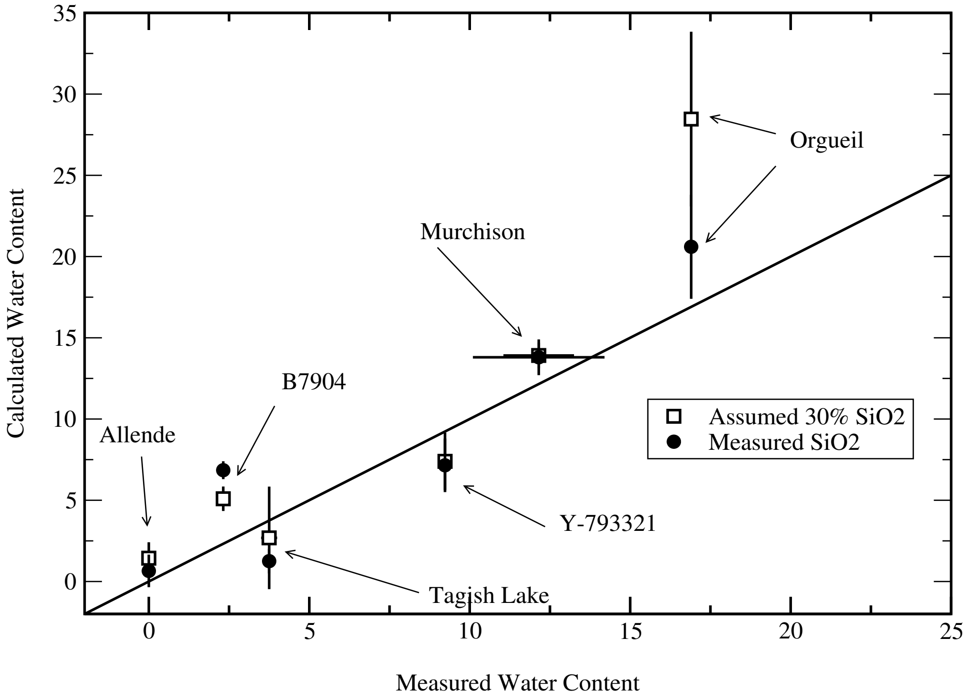

Figure 12: Using Equations 1 and 2 we determined the equivalent water content for six carbonaceous chondrites for which we have both geochemical data and reflectance spectra. The solid line is where predicted equals known values, and represents where the points should fall given perfect data and a perfect method. It is not a best fit line. The closed symbols use the known SiO_2 values from Jarosewich (199), the open symbols assume a SiO_2 concentration of 30%.